Supporting Information for "Consistent modelling of transport processes and travel times – coupling hydrologic processes with StorAge Selection functions "

Robin Schwemmle[1], Markus Weiler[1]

[1]Hydrology, Faculty of Environment and Natural Resources, University of Freiburg, Freiburg, Germany

Table of Contents

February 22, 2023, 4:12pm

1. Hydrologic processes and storages

Here, we provide the equations which were used to implement the hydrologic processes. Constant model parameters are listed in Table S2.

1.1. Surface storage

Storage capacity (i.e. available storage volume) of lower interception storage $S_{int-lower-tot}$ (mm) is land use dependent. Parameters used for grassland are shown in Table S1.

Leaf area index LAI (-):

$$LAI = \frac{S_{int-lower-tot}}{0.2} \tag{S1}$$

Fraction of ground cover $f_{ground-cover}$ (-):

$$f_{ground-cover} = 1 - 0.7^{LAI} \tag{S2}$$

1.2. Soil storage

Soil storage divides into a root zone layer rz (i.e. upper soil) and a subsoil layer ss (i.e. lower soil). The two soil layers share the same soil hydraulic parameters. However, absolute storage values are different due to different thickness of the layers. Root depth (z_{root}; mm) is shown in Table S1.

Soil hydraulic parameters are calculated with the Brooks-Corey scheme (Brooks & Corey, 1966). Pore size distribution parameter λ is calculated as:

$$\lambda = \frac{1}{\frac{\log\left(\frac{h_{fc}}{h_{pwp}}\right)}{\log\left(\frac{\omega_{fc}}{\omega_{pwp}}\right)}} \tag{S3}$$

where h_{fc} is soil water potential at field capacity (hPa; h_{fc}=63) and h_{pwp} is the soil water potential at permanent wilting point (hPa; h_{pwp}=15850)

Pore size disconnectedness index m:

$$m = b + \frac{a}{\lambda} \tag{S4}$$

where a and b are parameters with a fixed value of 2.

Salvucci exponent n (Salvucci, 1993):

$$n = \lambda \cdot a + b \tag{S5}$$

Effective soil water content at field capacity ω_{fc} (-):

$$\omega_{fc} = \frac{\theta_{fc}}{\theta_{sat}} \tag{S6}$$

where θ_{fc} is soil water content at field capacity (-) and θ_{sat} is soil water content at saturation (-).

Effective soil water content at permanent wilting point ω_{pwp} (-):

$$\omega_{pwp} = \frac{\theta_{pwp}}{\theta_{sat}} \tag{S7}$$

where θ_{pwp} is soil water content at permanent wilting point (-).

Effective soil water content ω (-):

$$\omega = \frac{\theta}{\theta_{sat}} \tag{S8}$$

Air entry value h_a (i.e. bubbling pressure, hPa):

$$h_a = \omega_{pwp}^{\frac{1}{\lambda}} \cdot (-1) \cdot h_{pwp} \tag{S9}$$

Soil water potential h (hPa):

$$h = \frac{h_a}{\omega^{\frac{1}{\lambda}}} \tag{S10}$$

Wetting front suction ψ_f (mm):

$$\psi_f = \frac{2 + 3\lambda}{(1 + 3\lambda) \cdot \frac{h_a}{2} \cdot (-10)} \tag{S11}$$

Hydraulic conductivity k (mm h-1):

$$k = \frac{k_s}{1 + \omega^m} \tag{S12}$$

Soil water content at $10^{2.7}$ hPa θ_{27} (-):

$$theta_{27} = \frac{h_a}{-10^{2.7}}^{\lambda_{bc} \cdot \theta_{sat}} \tag{S13}$$

Soil water content at 10^4 hPa θ_6 (-):

$$theta_4 = \frac{h_a}{-10^4}^{\lambda_{bc} \cdot \theta_{sat}} \tag{S14}$$

Soil water content at 10^6 hPa θ_6 (-):

$$theta_6 = \frac{h_a}{-10^6}^{\lambda_{bc} \cdot \theta_{sat}} \tag{S15}$$

Soil moisture deficit $\Delta\theta$ (-):

$$\Delta\theta = \theta_{sat} - \theta_{rz} \tag{S16}$$

1.3. Interception

Interception storage is represented by a bucket. The storage is filled by liquid and solid precipitation and spills if the storage is full. Interception at lower interception Storage $S_{int-lower}$ (mm Δt^{-1}):

Interception at lower interception Storage $S_{int-lower}$ (mm Δt^{-1}):

$$\frac{\Delta S_{int-lower}}{\Delta t} = \begin{cases} PREC(i) & PREC(i) \leq S_{tot-int-lower} - S_{int-lower} \\ S_{tot-int-lower} - S_{int-lower} & PREC(i) > S_{tot-int-lower} - S_{int-lower} \end{cases} \tag{S17}$$

1.4. Snow

Solid precipitation accumulates in the interception storage and at the land surface if air temperatures are below 0 °C. Snow melt occurs for air temperatures above 0 °C and is based on degree-day approach. Snow melt runoff is initiated if liquid storage of the snow cover (S_{snow-l}) exceeds the retention capacity of the snow cover. Retention capacity $S_{snow-ret}$ (mm):

$$S_{snow-ret} = \frac{10000}{\frac{100-r_{max}}{100}} \cdot swe \tag{S18}$$

where r_{max} is the retention factor of the snow cover (%) and swe is the snow water equivalent of the snow cover (mm).

Snow melt q_{snow} (mm):

$$q_{snow} = s_f \cdot (TA - TA_m) \cdot \Delta t \tag{S19}$$

where s_f is the degree-day factor (mm °C^{-1} h^{-1}), TA is the air temperature (°C), TA_m is equal to 0 °C and Δt is time step (h).

1.5. Evapotranspiration

The calculation of evapotranspiration requires daily potential evapotranspiration, which is calculated with the Makkink formula (Makkink, 1957):

$$\text{PET} = \frac{\Delta}{\Delta + \gamma} \cdot (c_1 \cdot \frac{r_s}{L(TA)} + c_2) \tag{S20}$$

with

$$L(TA) = c_L \cdot (28.4 - 0.028 \cdot TA) \tag{S21}$$

February 22, 2023, 4:12pm

:

where Δ is the saturation slope vapour pressure curve ($kPa\ °C^{-1}$) at TA, γ is the psychometric constant ($kPa\ °C^{-1}$), r_s is the measured or calculated solar radiation ($MJ\ m^{-2}\ day^{-1}$), L is the special heat of evaporation ($MJ\ m^{-2}\ mm^{-1}$), c_L is a conversion factor ($c_L = 0.0864$), $c1_{PET}$ is the Makkink coefficient (-) and $c2_{PET}$ is the Makkink coefficient (mm day^{-1}).

Actual evapotranspiration is energy-limited or water-limited, respectively. The evapotranspiration processes sequentially subtract from PET.

Evaporation from interception storage $EVAP_{int-lower}$ (mm Δt^{-1}):

$$EVAP_{int-lower} = \begin{cases} S_{int-lower} & PET_{res} > S_{int-lower} \\ PET_{res} & PET_{res} \leq S_{int-lower} \end{cases} \tag{S22}$$

Soil evaporation $EVAP_{soil}$ (mm Δt^{-1}) implemented with Stage I-Stage II approach (Or et al., 2013). Threshold between Stage I and Stage II is defined by readily evaporable water S_{rew}. Within Stage I capillary flow connects to soil surface (i.e. constant evaporation rate) whereas within Stage II capillary flow collapses (i.e. vapour diffusion rate).

$$EVAP = PET_{res} \cdot c_{evap} \tag{S23}$$

with

$$c_{evap} = \begin{cases} 1 - \frac{f_{ground-cover}}{max(f_{ground-cover})} & EVAP_d \leq S_{rew} \\ 1 - \frac{f_{ground-cover}}{max(f_{ground-cover})} \cdot \frac{S_{tew}-EVAP_d}{S_{tew}-S_{rew}} & S_{rew} < EVAP_d \leq S_{tew} \\ 0 & EVAP_d > S_{tew} \end{cases} \tag{S24}$$

where $EVAP_d$ is the cumulated soil evaporation since last rainfall (mm) and S_{tew} is the total evaporable water (mm)

$$S_{tew} = (\theta_{fc} - 0.5 \cdot \theta_{pwp}) \cdot z_{evap} \tag{S25}$$

$$S_{rew} = \begin{cases} 0.02 & \theta_{pwp} < 0.02 \\ \frac{\theta_{pwp}}{0.24} & \theta_{pwp} \geq 0.02 \& \theta_{pwp} \leq 0.24 \\ 0.24 & \theta_{pwp} > 0.24 \end{cases} \tag{S26}$$

$$z_{evap} = \frac{S_{rew}}{0.24} \cdot z_{evap-max} \tag{S27}$$

February 22, 2023, 4:12pm

where $z_{evap-max}$ is the maximum length of soil capillaries connected to the soil surface (mm; $z_{evap-max}$=150)

Transpiration $TRANSP$ (mm Δt^{-1}) with seasonally-variant transpiration coefficients c_{transp} and water stress coeffcient of transpiration $c_{transp-stress}$:

$$TRANSP = PET_{res} \cdot c_{transp} \tag{S28}$$

with

$$c_{transp} = \begin{cases} \frac{f_{ground-cover}}{max(f_{ground-cover})} & c_{transp-stress} \geq 1 \\ \frac{f_{ground-cover}}{max(f_{ground-cover})} \cdot c_{transp-stress} & c_{transp-stress} < 1 \end{cases} \tag{S29}$$

$$c_{transp-stress} = \frac{\theta - \theta_{pwp}}{f_{pwt} \cdot \theta_{fc} - \theta_{pwp}} \tag{S30}$$

where f_{pwt} is the fraction of plant water stress (-; f_{pwt}=0.75)

1.6. Infiltration

At the onset of rainfall or snow melt, we calculate event-specific parameters (e.g. soil moisture deficit $\Delta\theta$). For each event, we use two wetting fronts ($wf1$ and $wf2$). The second wetting front is active after a rainfall pause (i.e. calculation of event-specific parameters of $wf2$). $wf2$ is active while wetting front depth of $wf2$ is less than wetting front depth of $wf1$. In the following are the equations applied for dual-wetting front approach.

Total infiltration INF at time step t (mm Δt^{-1}):

$$INF = INF_{mat} + INF_{mp} + INF_{sc} \tag{S31}$$

Determining interval (i_s) when rainfall exceeds infiltrability within the current event:

$$i_s = \begin{cases} novalue & (PREC(i) - k_s \cdot \Delta t) \cdot \sum_{i=1}^{i} PREC(i) \leq k_s \cdot \Delta t \cdot \Delta\theta \cdot \psi_f \\ i & (PREC(i) - k_s \cdot \Delta t \cdot \sum_{i=1}^{i} PREC(i) > k_s \cdot \Delta t \cdot \Delta\theta \cdot \psi_f \end{cases} \tag{S32}$$

February 22, 2023, 4:12pm

where $PREC$ is precipitation (mm Δt^{-1}), k_s is the saturated hydraulic conductivity of

the soil matrix, $\Delta\theta$ is the soil moisture deficit (-) and ψ_f is the wetting front suction (mm)

Threshold rainfall intensity $PREC_{gr}$ (mm Δt^{-1}):

$$PREC_{gr} = k_s \cdot \Delta t \cdot \left(\frac{\Delta\theta \cdot \psi_f}{\sum_{i=1}^{i_s-1} PREC(i)} + 1 \right) \tag{S33}$$

$$i_s = \begin{cases} (i_s - 1) \cdot \Delta t & PREC(i_s) < PREC_{gr} \\ (i_s - 1) \cdot \Delta t + \frac{k_s \cdot \Delta t \cdot \Delta\theta \cdot \psi_f}{PREC(i_s) \cdot (PREC(i_s) - k_s \cdot \Delta t)} \frac{\Delta t}{PREC(i_s)} \sum_{v=1}^{i_s-1} PREC_v & PREC(i_s) \geq PREC_{gr} \end{cases} \tag{S34}$$

Infiltration at time step of saturation F_s (mm Δt^{-1}):

$$F_s = \frac{k_s \cdot \Delta t \cdot \theta_d \cdot \psi_f}{PREC(i_s) - k_s \cdot \Delta t} \tag{S35}$$

Matrix infiltration INF_{mat} at time step t (mm Δt^{-1}):

$$INF_{mat} = \begin{cases} z_0 \cdot & z_0 \leq INF_{mp-pot} \\ INF_{mat-pot} & z_0 > INF_{mp-pot} \end{cases} \tag{S36}$$

where z_0 is the surface ponding (mm; i.e. residual rainfall after interception or snow melt).

with potential matrix infiltration at time step t $INF_{mat-pot}$ (mm Δt^{-1}):

$$INF_{mat-pot} = \begin{cases} PREC(t) & t_s \geq t \\ PREC(t) \cdot (t_s - t - \Delta t) + \frac{k_s}{2}(1 + \frac{1+\frac{2B}{A}}{\sqrt{1+\frac{4B}{A}+\frac{4F_s^2}{A^2}}}) & t - \Delta t < t_S < t \\ \frac{k_s}{2}(1 + \frac{1+\frac{2B}{A}}{\sqrt{1+\frac{4B}{A}+\frac{4F_s^2}{A^2}}}) & t_s < t \end{cases} \tag{S37}$$

with auxiliary variables:

$$A = K_S \cdot (t - t_s) \tag{S38}$$

$$B = F_s + 2 \cdot \Delta\theta \cdot \psi_f \tag{S39}$$

Wetting front depth z_{wf} (mm):

$$z_{wf} = \frac{\sum_i^i INF_{mat}(i)}{\Delta\theta} \tag{S40}$$

February 22, 2023, 4:12pm

where i_e is interval of the event start.

Macropore infiltration INF_{mp} at time step t (mm Δt^{-1}) following Weiler (2005):

$$INF_{mp} = \begin{cases} z_0 \cdot (1 - e^{-(\frac{\rho_{mpv}}{82})^{0.887}}) & 0 < z_0 \cdot (1 - e^{-(\frac{\rho_{mpv}}{82})^{0.887}}) \leq INF_{mp-pot} \\ INF_{mp-pot} & z_0 \cdot (1 - e^{-(\frac{\rho_{mpv}}{82})^{0.887}}) > INF_{mp-pot} \end{cases} \qquad (S41)$$

where z_0 is the surface ponding (mm; i.e. matrix infiltration excess).

with potential macropore infiltration INF_{mp-pot} at time step t (mm Δt^{-1})

$$INF_{mp-pot} = \pi \cdot (y_{mp}(t)^2 - y_{mp}(t - \Delta t)^2) \cdot \rho_{mpv} \cdot \frac{\Delta z_{mp} \cdot \Delta \theta}{\Delta t} \qquad (S42)$$

where ρ_{mpv} is density of vertical macropores (m^2) and Δz_{mp} depth of non-saturated macropore (mm)

Radial distance of the macropore wetting front y_{mp} (mm):

$$y_{mp} = \frac{1}{2} \cdot \frac{b^{(1/3)}}{\Delta \theta} + \frac{1}{2} \cdot \frac{a}{b^{(1/3)}} + \frac{1}{2} \cdot r_{mp} \qquad (S43)$$

$$a = \Delta \theta \cdot r_{mp}^2 \qquad (S44)$$

$$b = r \cdot \Delta \theta \cdot (12c - a + 2\sqrt{6} \cdot \sqrt{c \cdot (6c - a)}) \qquad (S45)$$

$$c = t_{mp} \cdot k_s \cdot \psi_s \qquad (S46)$$

Duration of macropore infiltration t_{mp} ($y_{mp}=r_{mp}$ at time t=0)

$$t_{mp} = \frac{\Delta \theta}{k_s \cdot \Psi_s \cdot r_{mp}} \cdot (\frac{y_{mp}^3}{3} - \frac{y_{mp}^2 r}{2} - \frac{r_{mp}^3}{6}) \qquad (S47)$$

where r_{mp} is the radius of the macropore (mm; $r_{mp}=2.5$). Macropore infiltration stops if z_{wf} is greater than l_{mpv}.

Shrinkage crack infiltration INF_{cs} at time step t (mm Δt^{-1}) following Steinbrich, Leistert, and Weiler (2016):

$$INF_{sc} = \begin{cases} z_0 & z_0 \leq INF_{sc-pot} \\ INF_{sc-pot} & z_0 > INF_{sc-pot} \end{cases} \qquad (S48)$$

:

where z_0 is the surface ponding (mm; i.e. macropore infiltration excess).

Potential shrinkage crack infiltration INF_{sc-pot} at time step t (mm Δt^{-1}):

$$INF_{sc-pot} = 2 \cdot l_{sc} \cdot (y_{sc}(t) - y_{sc}(t - \Delta t)) \cdot \frac{\Delta z_{sc} \cdot \Delta \theta}{\Delta t} \qquad \text{(S49)}$$

where l_{sc} is the horizontal length of shrinkage cracks (mm m^{-2}) and Δz_{sc} is the depth of non-saturated shrinkage crack (mm)

Horizontal distance of the shrinkage crack wetting front y_{sc} (mm):

$$y_{sc}(t) = \sqrt{\frac{2 \cdot k_s \cdot \Psi_s \cdot t_{sc}}{\Delta \theta}} \qquad \text{(S50)}$$

$$t_{sc} = \frac{y_{sc}(t - \Delta t)^2 \cdot \Delta \theta}{2 \cdot k_s \cdot \psi_s} \qquad \text{(S51)}$$

Calculation of depth of shrinkage cracks z_{sc} at beginning of event:

$$z_{sc} = \begin{cases} 700 \cdot clay & \theta_{rz} < \theta_4 \\ 700 \cdot clay \cdot (1 - \frac{\theta_{rz}}{\theta_{27}-\theta_4}) & \theta_4 \leq \theta_{rz} \leq \theta_{27} \\ 0 & \theta_{rz} > \theta_{27} \end{cases} \qquad \text{(S52)}$$

with clay content of soil $clay$ (-)

$$clay = \frac{clay_{max} \cdot (\theta_6 - clay_{min})}{0.3} \qquad \text{(S53)}$$

where $clay_{min}$ is the lower limit of clay content (-; $clay_{min}$=0.01) and $clay_{max}$ is the upper limit of clay content (-; $clay_{max}$=0.71). INF_{sc} occurs only if shrinkage cracks are available and stops if z_{wf} is greater than z_{sc}.

1.7. Surface runoff

Hortonian surface runoff q_{HOF} at time step t (mm Δt^{-1}):

$$q_{HOF} = \begin{cases} PREC - INT - INF & PREC - INT - INF > 0 \\ 0 & PREC - INT - INF \leq 0 \end{cases} \qquad \text{(S54)}$$

Saturation surface runoff q_{HOF} at time step t (mm Δt^{-1}):

$$q_{SOF} = \begin{cases} S_{soil} - S_{sat-soil} & S_{soil} - S_{sat-soil} > 0 \\ 0 & S_{soil} - S_{sat-soil} \leq 0 \end{cases} \qquad \text{(S55)}$$

February 22, 2023, 4:12pm

where $S_{sat-soil}$ is soil water content at saturation (mm) and S_{soil} and soil water content at time step t (mm).

1.8. Percolation/Capillary rise

Vertical flux q_v (mm Δt^{-1}):

$$q_v = \begin{cases} \frac{(z_{sat}/h_a)^{-n}-(h/h_a)^{-n}}{1+(h/h_a)^{-n}+(n-1)(z_{sat}/h_a)^{-n}} & z_{gw} \leq 10 \\ \frac{(z_{sat}/h_a)^{-n}}{1+(n-1)(z_{sat}/h_a)^{-n}} & z_{gw} > 10 \end{cases} \quad (S56)$$

where z_{gw} is the depth of groundwater table (m). For $q_v < 0$ soil water moves in downward direction and for with $q_v > 0$ soil water moves in upward direction.

Percolation q_{perc} (mm Δt^{-1}):

$$q_{perc} = \begin{cases} k_s & z_{sat} > 0 \\ q_v \cdot (-1) & q_v < 0 \& z_{sat} = 0 \\ 0 & q_v \geq 0 \& z_{sat} = 0 \end{cases} \quad (S57)$$

where z_{sat} is saturation water level at the soil-bedrock interface (mm).

Percolation might be limited by permeability of bedrock (k_f, mm Δt^{-1}), if q_{perc} exceeds k_f.

Saturation water level z_{sat} (mm) rises while saturation from top is connected to the bedrock interface:

$$z_{sat} = \begin{cases} \frac{S_{lp-ss}}{\theta_{ac}} & \frac{S_{lp-ss}}{\theta_{ac}} \geq z_{nomp} \\ z_{sat} & \frac{S_{lp-ss}}{\theta_{ac}} < z_{nomp} \end{cases} \quad (S58)$$

with thickness without macropores z_{nomp} (mm):

$$z_{nomp} = \begin{cases} 0 & z_{soil} - l_{mpv} - z_{sat} < 0 \\ z_{soil} - l_{mpv} - z_{sat} & z_{soil} - l_{mpv} - z_{sat} > 0 \end{cases} \quad (S59)$$

where S_{lp-ss} is soil water content in large pores of subsoil (mm). z_{sat} is reduced by percolation q_{perc}.

Capillary rise q_{cpr} (mm Δt^{-1}):

$$q_{cpr} = \begin{cases} 0 & q_v < 0 \\ q_v & q_v \geq 0 \& z_{sat} = 0 \end{cases} \quad (S60)$$

February 22, 2023, 4:12pm

2.   RoGeR - Monte Carlo analysis and Sensitivity analysis

Dotty plots of hydrologic Monte Carlo simulations are shown in Figure S3. Since best parameter values are not close to the parameter boundaries, the Monte Carlo approach provides a robust and hydrologically coherent estimation of the parameters. Sobol' indices of hydrologic Monte Carlo simulations are shown in Figure S8.

In addition to the single-parameter power law distribution function (see equation (7)), we implemented SAS with a dual-parameter distribution function (Figure S6) using the Kumaraswamy distribution function (Kumaraswamy, 1980):

$$\Omega_Q(T,t) = 1 - (1 - (P_s(T,t)^a)^b) \tag{S61}$$

with two parameters a and b, the Kumaraswamy distribution function provides a greater flexibility than a power law distribution function.

3.   RoGeR - Model evaluation per hydrologic year

For further evaluation, we cumulated values for each year and compared hydrologic observations with best 100 hydrologic simulations. The results are shown in Figures S11, S12 and S13.

4.   HYDRUS-1D - Model setup and dotty plots of Monte Carlo simulations

We use HYDRUS-1D with dual-porosity domain for which transfer is proportional to the effective saturation (Šimůnek et al., 2016). The model setup is summarized by Table S3. The soil is represented by a single layer. Input data comes with a daily temporal resolution. We modified precipitation input with the snow and interception routine of RoGeR. The partition of potential evapotranspiration in potential transpiration and potential soil evap-

oration is based on ground cover root depth (i.e. same values is for RoGeR). The potential root water uptake distribution is calculates as proposed by Hoffman and Van Genuchten (1983). Initial conditions for $\delta^{18}O$ of soil water are derived by a warmup period of 2 years (1997-1998). Initial soil water potentials are set to 100 hPa. Galerkin Finite Element method (Δz=2 cm) was used for the spatial discretization and Crank-Nicholson approach (Δt=0.01 day) was used for the temporal discretization. Convergence criteria is an absolute volumetric water tolerance of 0.001 for the unsaturated nodes and a pressure head tolerance of 1 cm for the saturated nodes.

In order to calculate forward travel time distributions and residence time distributions, we followed the approach described in Brinkmann et al. (2018). Since forward travel time distributions and backward travel time distributions relate to each other (Benettin et al., 2015), we calculate from forward travel time distributions the corresponding backward travel time distributions to enable a comparison with RoGeR. In order to avoid truncated travel time distributions, we skipped the first 1000 days to estimate backward travel time distributions.

We run 30 000 Monte Carlo simulations with HYDRUS-1D to derive a well performing parameter set which is used for benchmark simulations (see Table S3). Dotty plots of Monte Carlo simulations with HYDRUS-1D are exhibited in Figure S14. From the Monte Carlo simulations, we selected the best performing parameter set according to equation (10). This procedures provides robust and realistic parameter set (see Figure S14).

5. HYDRUS-1D - Soil water, $\delta^{18}O$ of soil water and mean residence time of soil water

The temporal evolution of soil water content (Figure S15) and $\delta^{18}O$ (Figure S16) in soil water simulated with HYDRUS-1D reveals that events with little precipitation stuck within the upper soil (≤ 40 cm).

References

Benettin, P., Rinaldo, A., & Botter, G. (2015). Tracking residence times in hydrological systems: forward and backward formulations. *Hydrological Processes*, *29*(25), 5203-5213. Retrieved from `https://onlinelibrary.wiley.com/doi/abs/10.1002/hyp.10513` doi: https://doi.org/10.1002/hyp.10513

Brinkmann, N., Seeger, S., Weiler, M., Buchmann, N., Eugster, W., & Kahmen, A. (2018). Employing stable isotopes to determine the residence times of soil water and the temporal origin of water taken up by fagus sylvatica and picea abies in a temperate forest. *New Phytologist*, *219*(4), 1300-1313. Retrieved from `https://nph.onlinelibrary.wiley.com/doi/abs/10.1111/nph.15255` doi: https://doi.org/10.1111/nph.15255

Brooks, R. H., & Corey, A. T. (1966). Properties of porous media affecting fluid flow. *Journal of the Irrigation and Drainage Division*, *92*, 61-90.

Hoffman, G. J., & Van Genuchten, M. T. (1983). Soil properties and efficient water use: Water management for salinity control. *Limitations to Efficient Water Use in Crop Production*, 73-85.

Kumaraswamy, P. (1980). A generalized probability density function for double-bounded random processes. *Journal of Hydrology*, *46*(1), 79-88. Retrieved from `https://`

www.sciencedirect.com/science/article/pii/0022169480900360 doi: https://doi.org/10.1016/0022-1694(80)90036-0

Makkink, G. F. (1957). Testing the penman formula by means of lysimeters. *Journal of the Institution of Water Engineers*, *11*, 277-288.

Or, D., Lehmann, P., Shahraeeni, E., & Shokri, N. (2013). Advances in soil evaporation physics—a review. *Vadose Zone Journal*, *12*(4), vzj2012.0163. Retrieved from https://acsess.onlinelibrary.wiley.com/doi/abs/10.2136/vzj2012.0163 doi: https://doi.org/10.2136/vzj2012.0163

Salvucci, G. D. (1993). An approximate solution for steady vertical flux of moisture through an unsaturated homogeneous soil. *Water Resources Research*, *29*(11), 3749-3753. Retrieved from https://agupubs.onlinelibrary.wiley.com/doi/abs/10.1029/93WR02068 doi: https://doi.org/10.1029/93WR02068

Steinbrich, A., Leistert, H., & Weiler, M. (2016, Nov 02). Model-based quantification of runoff generation processes at high spatial and temporal resolution. *Environmental Earth Sciences*, *75*(21), 1423. Retrieved from https://doi.org/10.1007/s12665-016-6234-9 doi: https://doi.org/10.1007/s12665-016-6234-9

Weiler, M. (2005). An infiltration model based on flow variability in macropores: development, sensitivity analysis and applications. *Journal of Hydrology*, *310*(1), 294-315. Retrieved from https://www.sciencedirect.com/science/article/pii/S0022169405000132 doi: https://doi.org/10.1016/j.jhydrol.2005.01.010

Šimůnek, J., van Genuchten, M. T., & Šejna, M. (2016). Recent developments and applications of the hydrus computer software packages. *Vadose Zone Journal*, *15*(7), vzj2016.04.0033. Retrieved from https://acsess.onlinelibrary.wiley.com/doi/
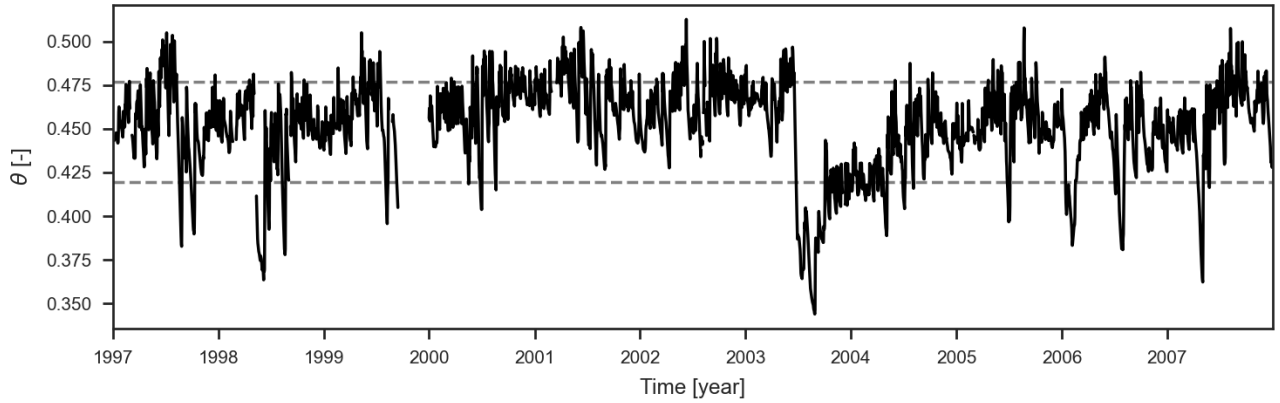
Figure S1. Moving average (5 days) of observed soil water content to define antecedent soil moisture conditions.

Table S1. Surface parameters and root depth of RoGeR for land use class grass (`lu_id`=8)

	Jan	Feb	Mar	Apr	May	Jun	Jul	Aug	Sep	Oct	Nov	Dec
$f_{ground-cover}$ [-]	0.51	0.51	0.66	0.76	0.83	0.83	0.83	0.83	0.83	0.66	0.59	0.51
LAI [-]	2	2	3	4	5	5	5	5	5	3	2.5	2
$S_{int-lower-tot}$ [mm]	0.4	0.4	0.6	0.8	1	1	1	1	1	0.6	0.5	0.4
z_{root} [mm]	400	400	400	400	400	400	400	400	400	400	400	400

Table S2. Constant model parameters of RoGeR

Constant parameters		Unit	Value
Degree-day factor	s_f	-	3
Threshold air temperature of freeze/melt	ta_{fm}	degC	0
Retention capacity of liquid water in snow cover	r_{max}	%	30
Threshold duration of no rainfall/snow melt	$t_{end-event}$	h	5
Threshold for classification of heavy rainfall event	hpi	mm 10 min^{-1}	5
Radius of macropores	r_{mp}	mm	2.5
Maximum length of shrinkage cracks	l_{sc}	mm m^{-2}	10000
Parameter for Brooks-Corey	a_{bc}	-	2
Parameter for Brooks-Corey	b_{bc}	-	2
Fraction for plant water stress	f_{pwt}	-	0.75

February 22, 2023, 4:12pm
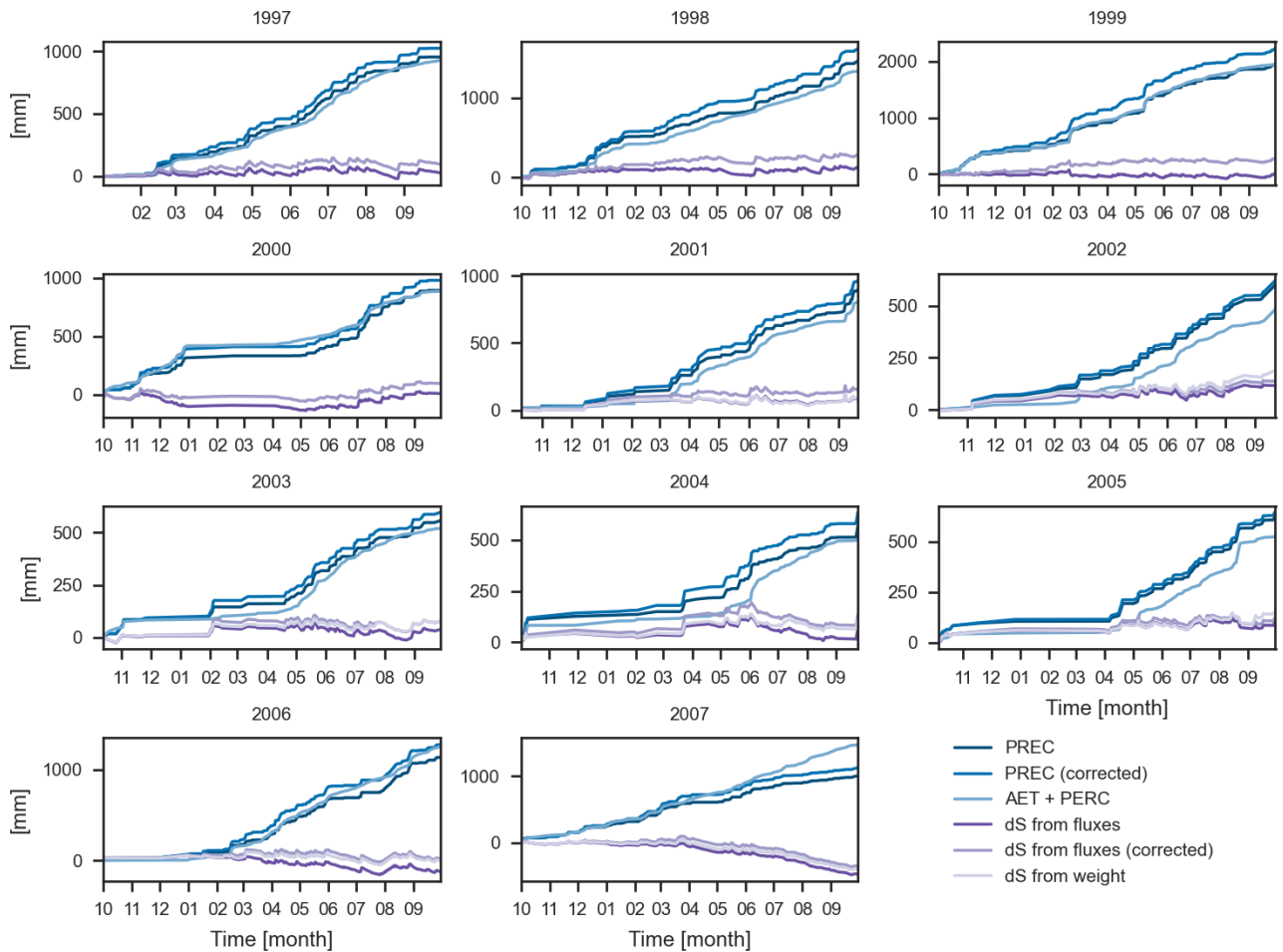
Figure S2. Cumulated values per hydrologic year of measured precipitation, evapotranspiration, storage change and lysimeter seepage at Rietholzbach lysimeter from 1997 to 2007.
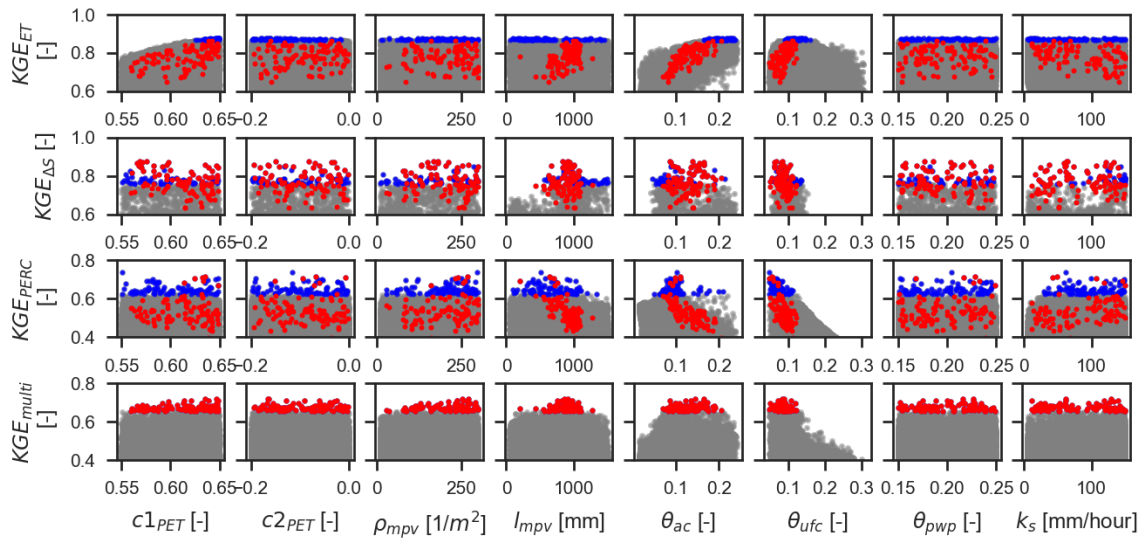
Figure S3. Dotty plots of Monte Carlo simulations with RoGeR. Red dots indicate best 100 simulations according to E_{multi} and blue dots show best 100 simulations for the corresponding metric.
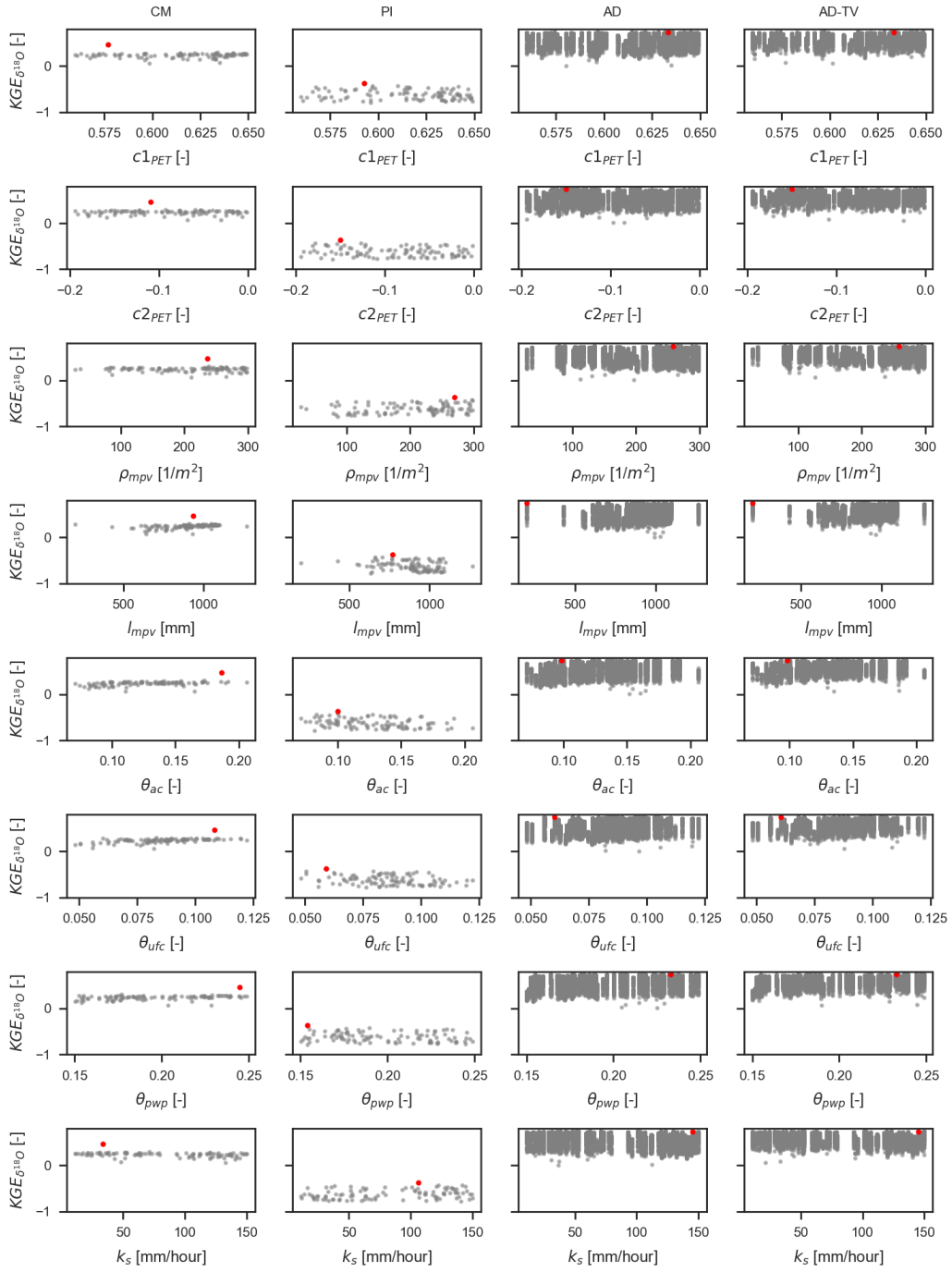
Figure S4. Dotty plots of hydrologic model parameters for Monte Carlo $\delta^{18}O$ simulations with RoGeR. Red dot indicates best simulations according to KGE.
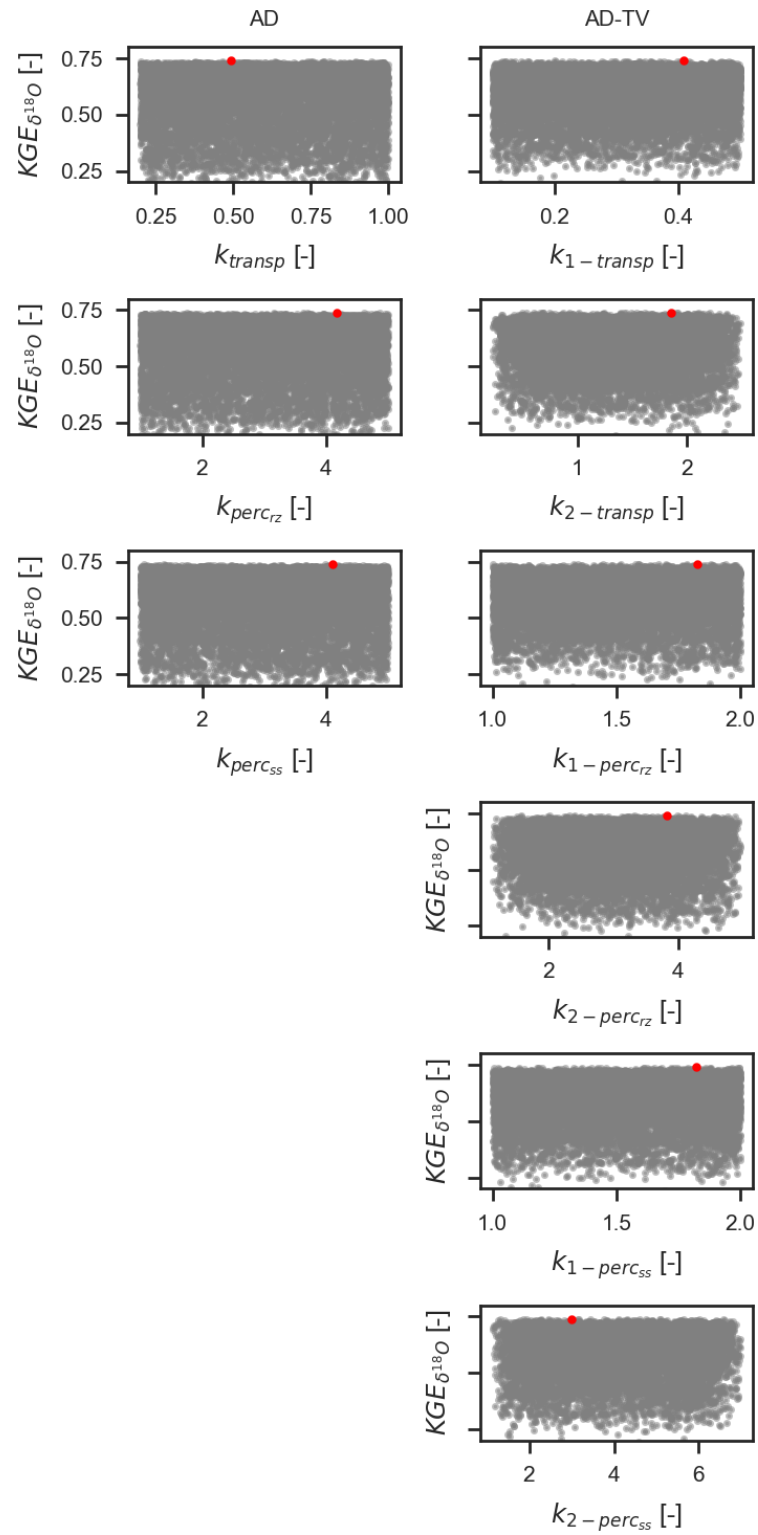
Figure S5.   Dotty plots of SAS parameters for Monte Carlo $\delta^{18}O$ simulations with RoGeR. The red dot indicates best simulations according to KGE.
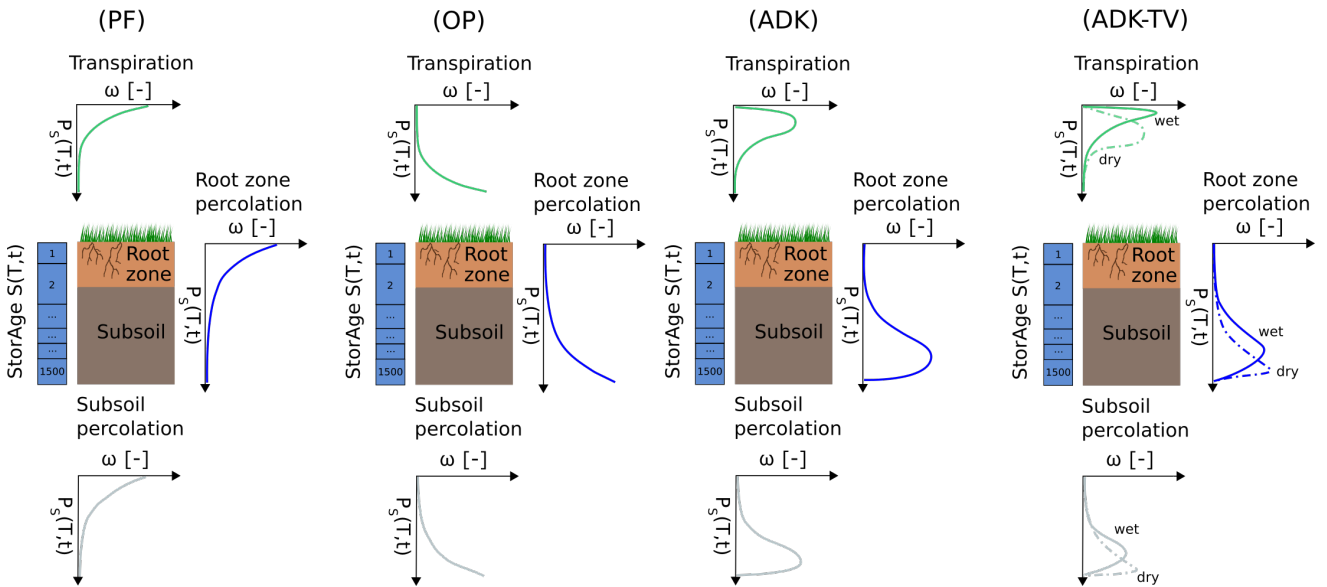
Figure S6. Additional transport model structures: Preferential transport model (PF), Old-preference transport model (OP), Advection-dispersion transport model using a Kumaraswamy distribution function (ADK) and Advection-dispersion transport model with time-variant SAS parameters using a Kumaraswamy distribution function (ADK-TV).
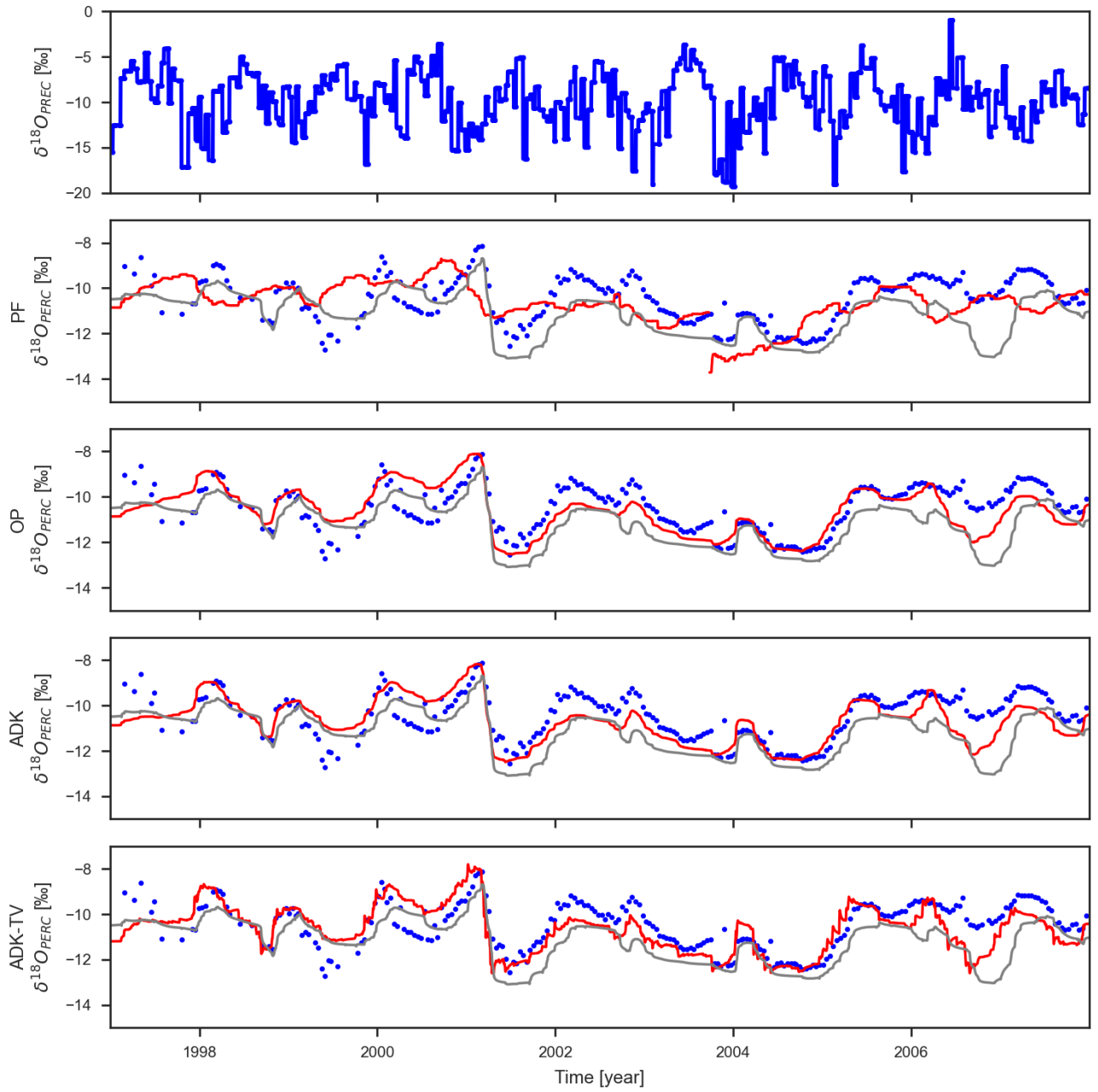
Figure S7. Observed $\delta^{18}O$ in precipitation and observed (blue) and simulated $\delta^{18}O$ in percolation with RoGeR (red) and HYDRUS-1D (grey). Values are shown for different model structures (see Figure S6).

:
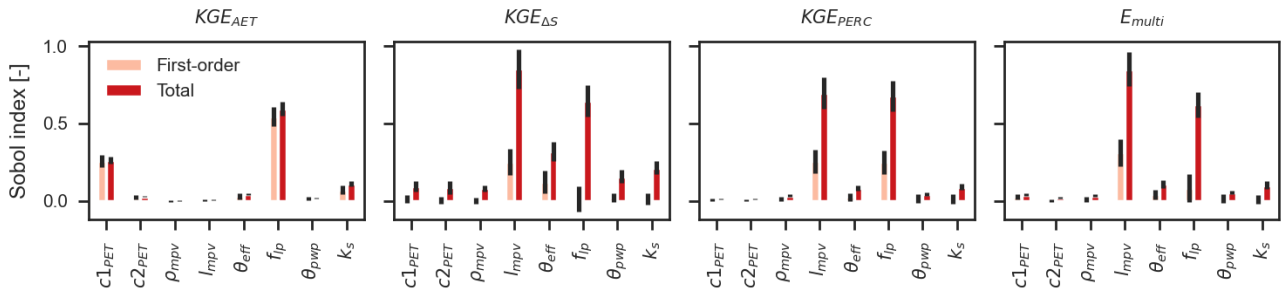
Figure S8. Sobol' indices of hydrologic model parameters calculated for KGE of evapotranspiration, storage change, percolation and multi-objective criteria.
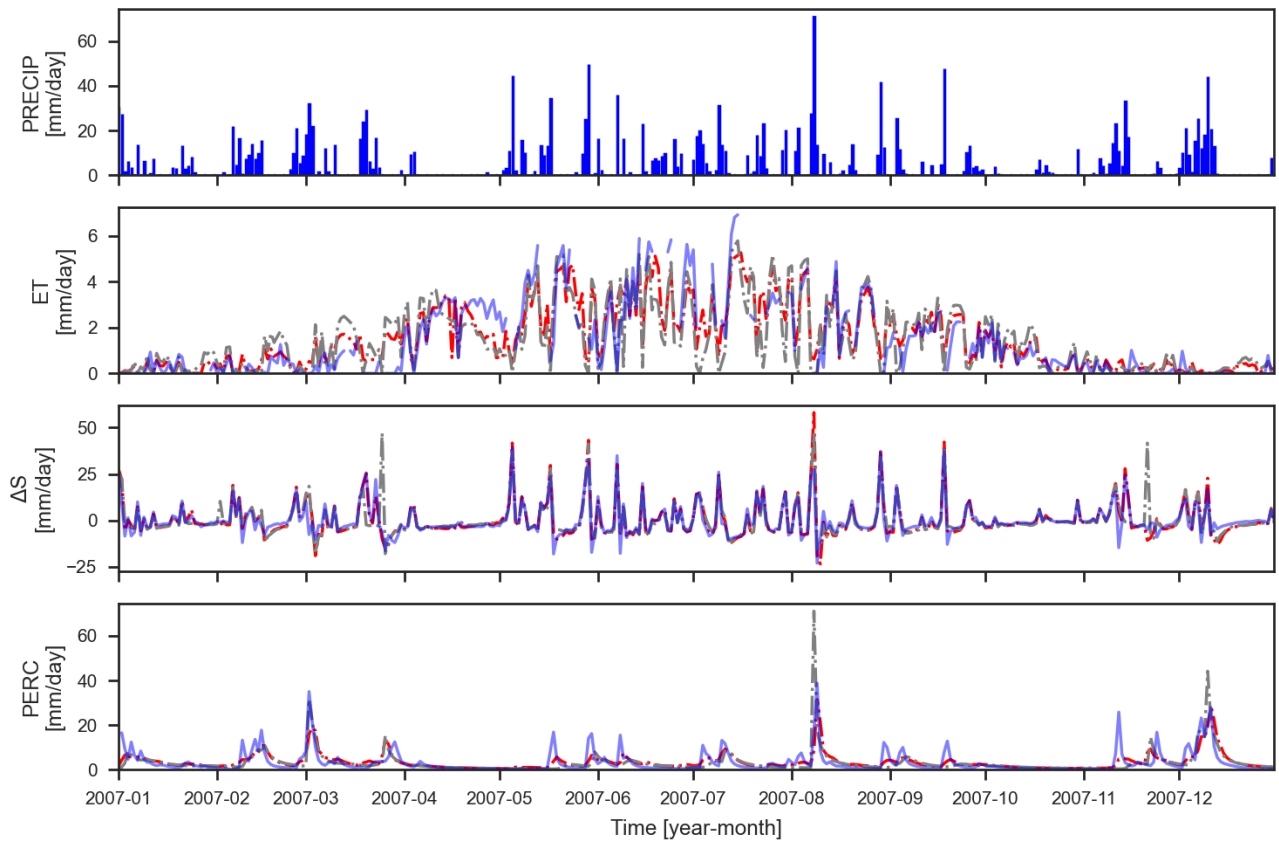
Figure S9. Comparison of observed (blue), simulated values with RoGeR (red) and simulated values with HYDRUS-1D (grey) in year 2007. Simulated values are shown for best parameter set according to E_{multi} or KGE_{multi}, respectively.

February 22, 2023, 4:12pm
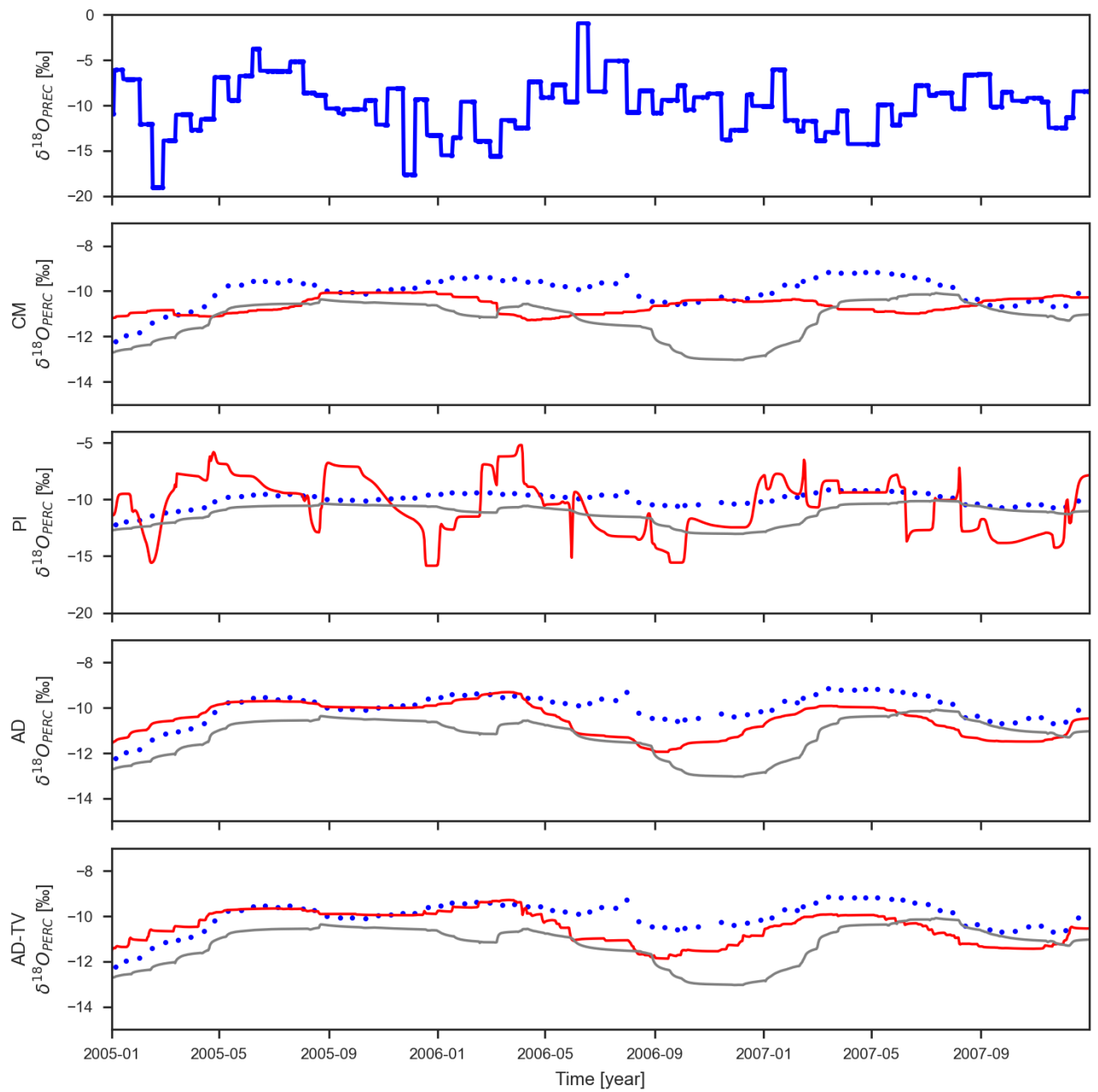
Figure S10. Comparison of observed (blue) and simulated $\delta^{18}O$ in percolation (red) in years 2005-2007. Simulated values are shown for best parameter set according to $KGE_{\delta^{18}O}$. The grey line indicates the benchmark simulation with HYDRUS-1D.

February 22, 2023, 4:12pm
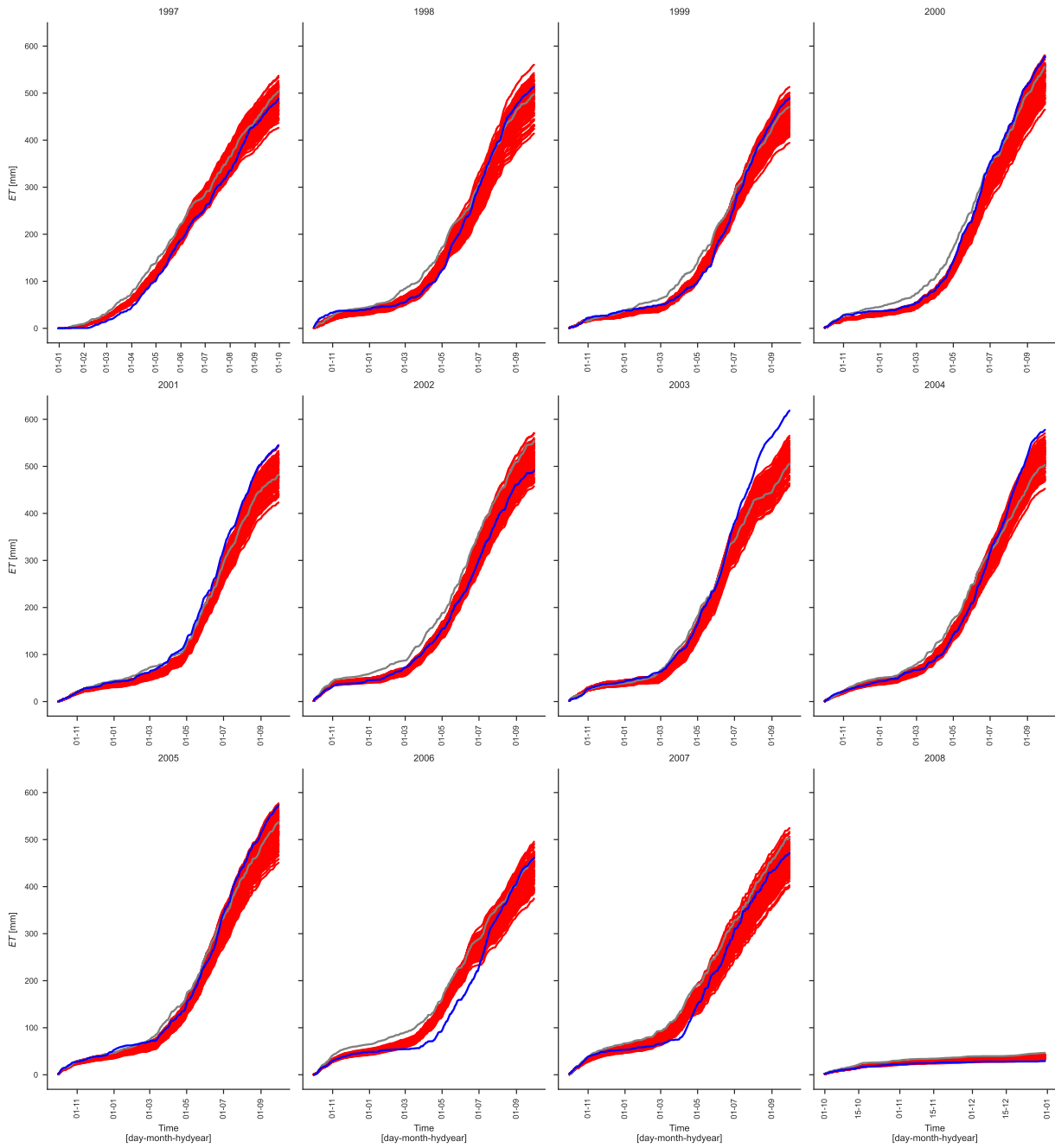
Figure S11. Comparison of cumulated observed evapotranspiration (blue) and simulated evapotranspiration (red) shown for best 100 simulations according to E_{multi}. Values are cumulated for each hydrologic year. The grey line indicates the benchmark simulation with HYDRUS-1D.

February 22, 2023, 4:12pm
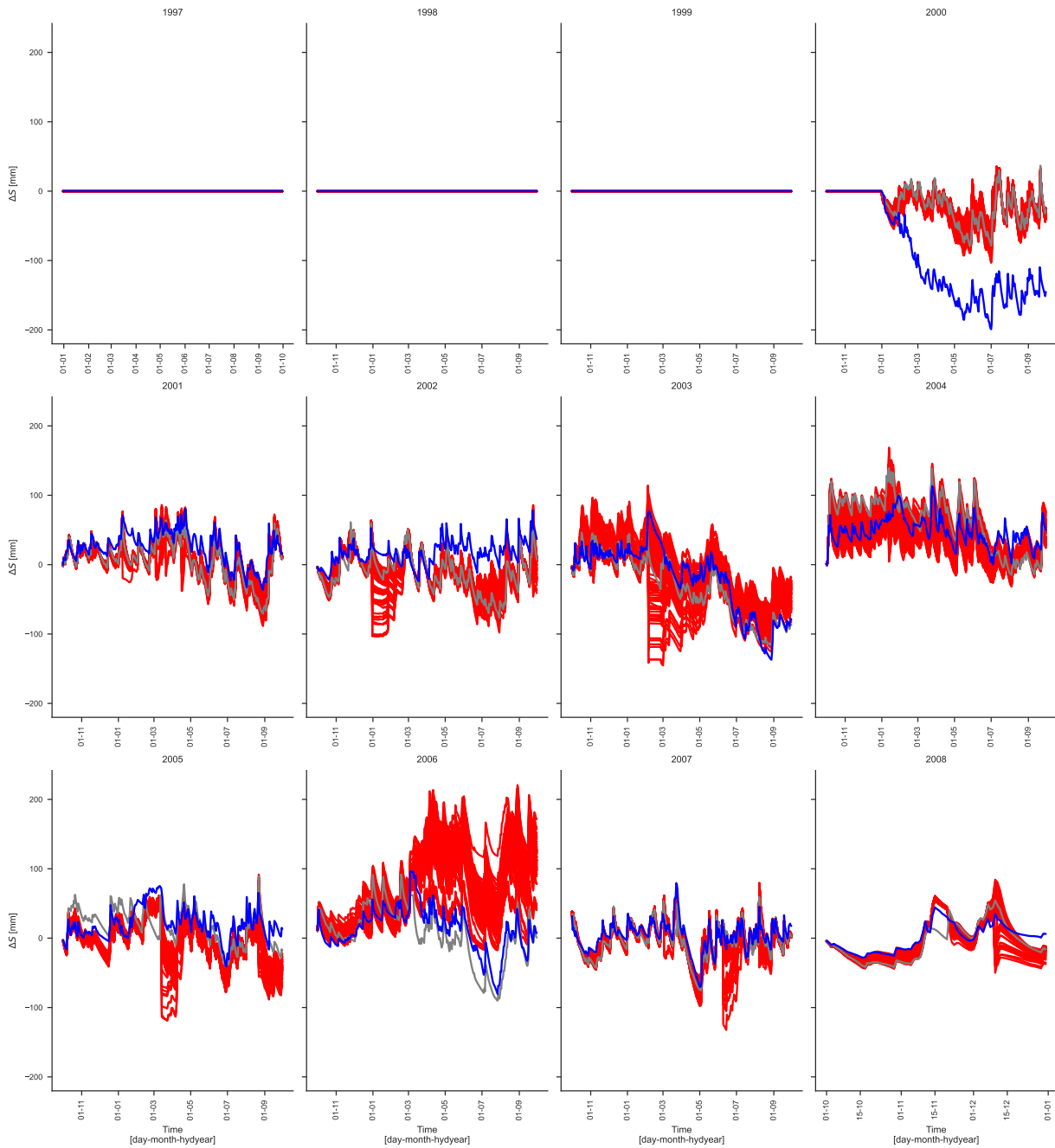
Figure S12. Comparison of cumulated storage change (blue) and simulated storage change (red) shown for best 100 simulations according to E_{multi}. Values are cumulated for each hydrologic year. The grey line indicates the benchmark simulation with HYDRUS-1D. From 1997 to 1999 no observations on storage change were available.

February 22, 2023, 4:12pm
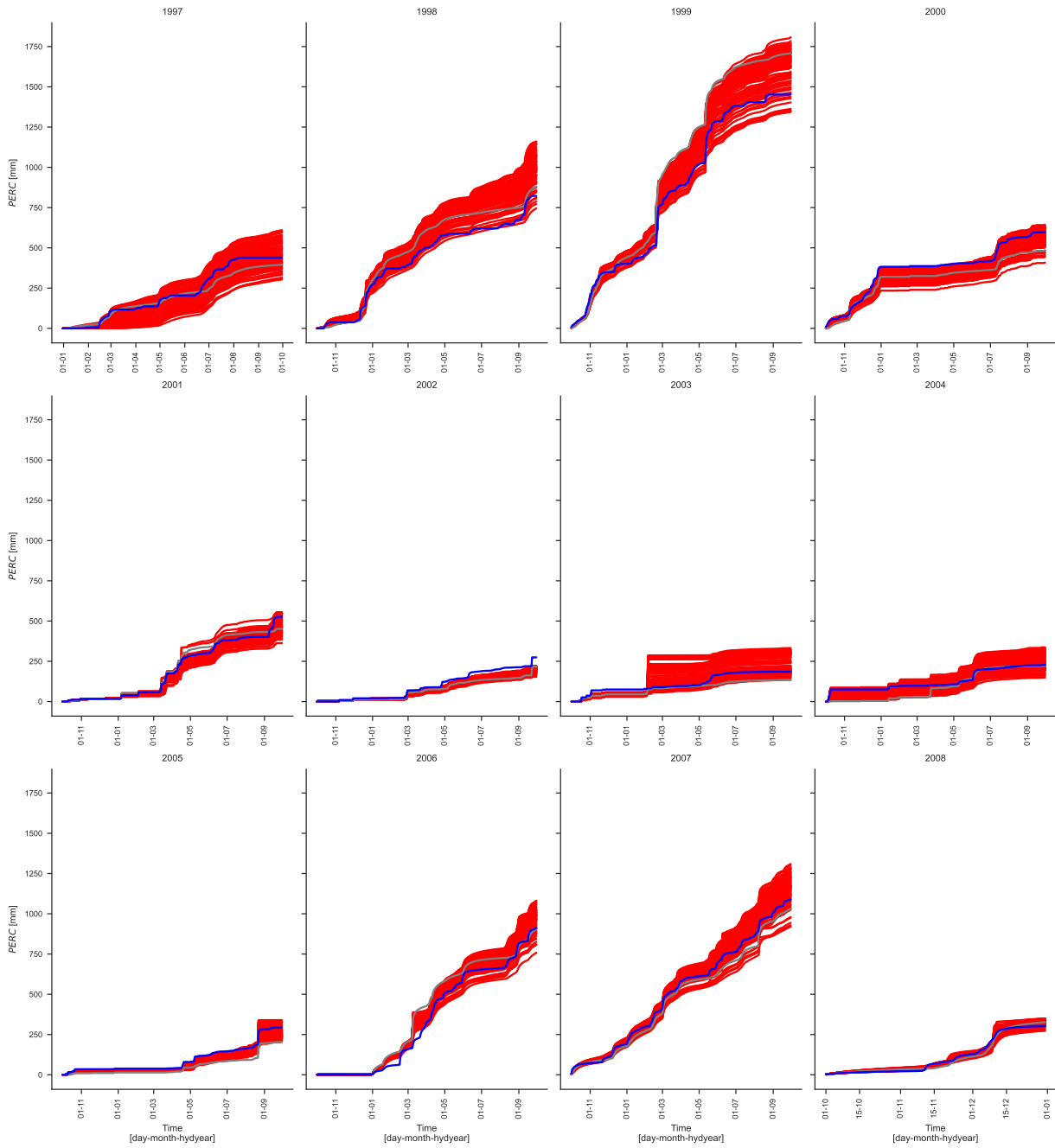
Figure S13. Comparison of cumulated percolation (blue) and simulated percolation (red) shown for best 100 simulations according to E_{multi}. Values are cumulated for each hydrologic year. The grey line indicates the benchmark simulation with HYDRUS-1D.
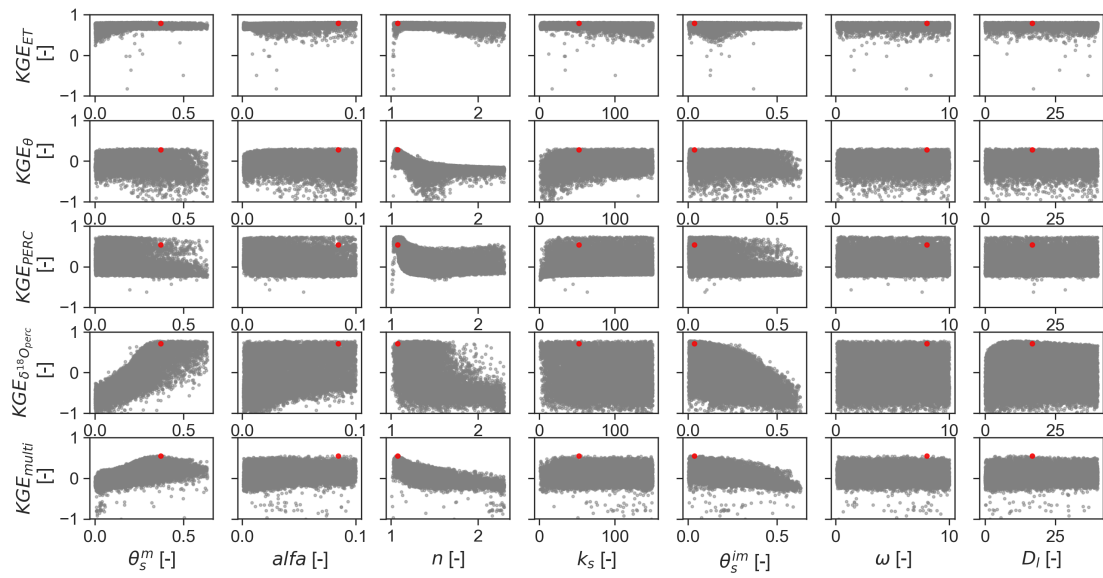
Figure S14. Dotty plots of Monte Carlo simulations with HYDRUS-1D. Red dot indicates best simulation according to KGE_{multi}.
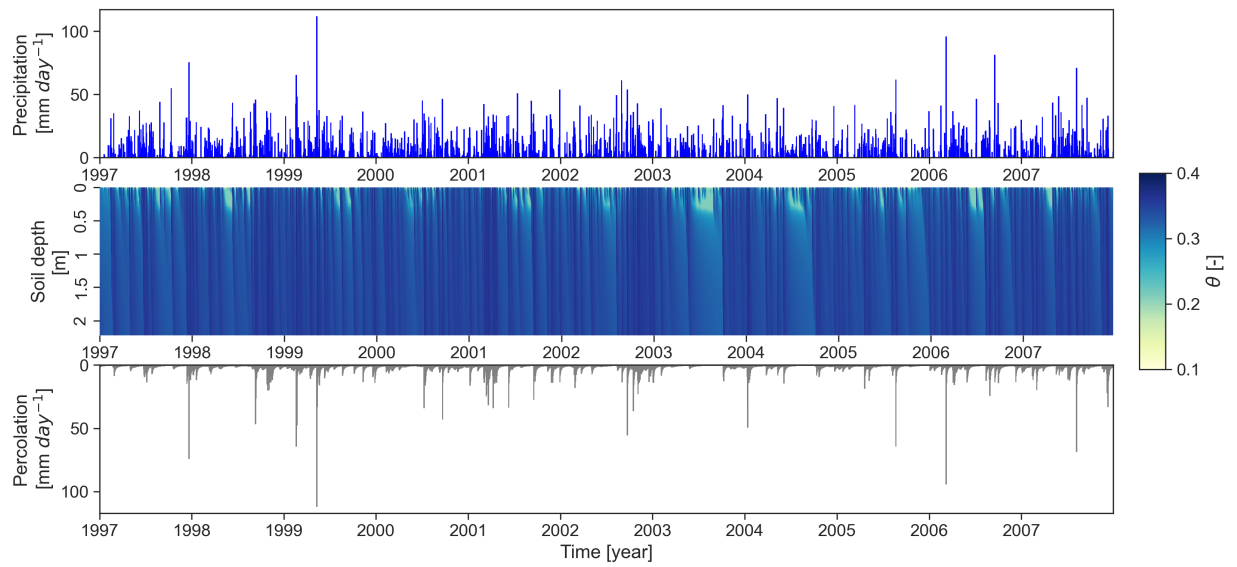
Figure S15. Precipitation, simulated soil water content and simulated percolation with HYDRUS-1D.
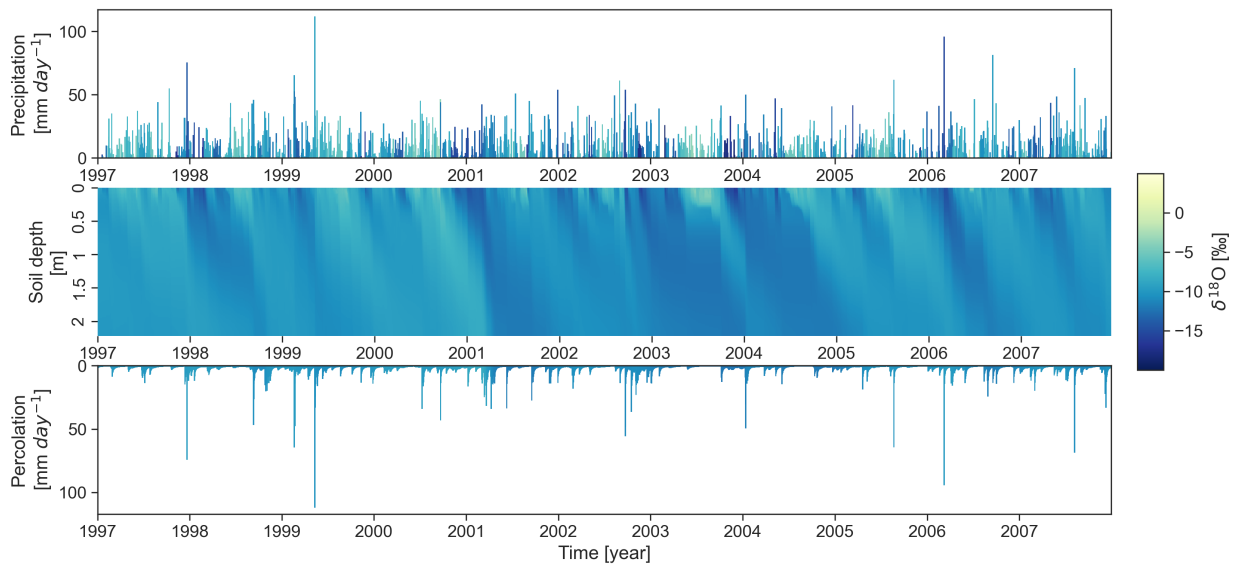
Figure S16. $\delta^{18}O$ of precipitation, simulated $\delta^{18}O$ of soil water and $\delta^{18}O$ of simulated percolation with HYDRUS-1D.
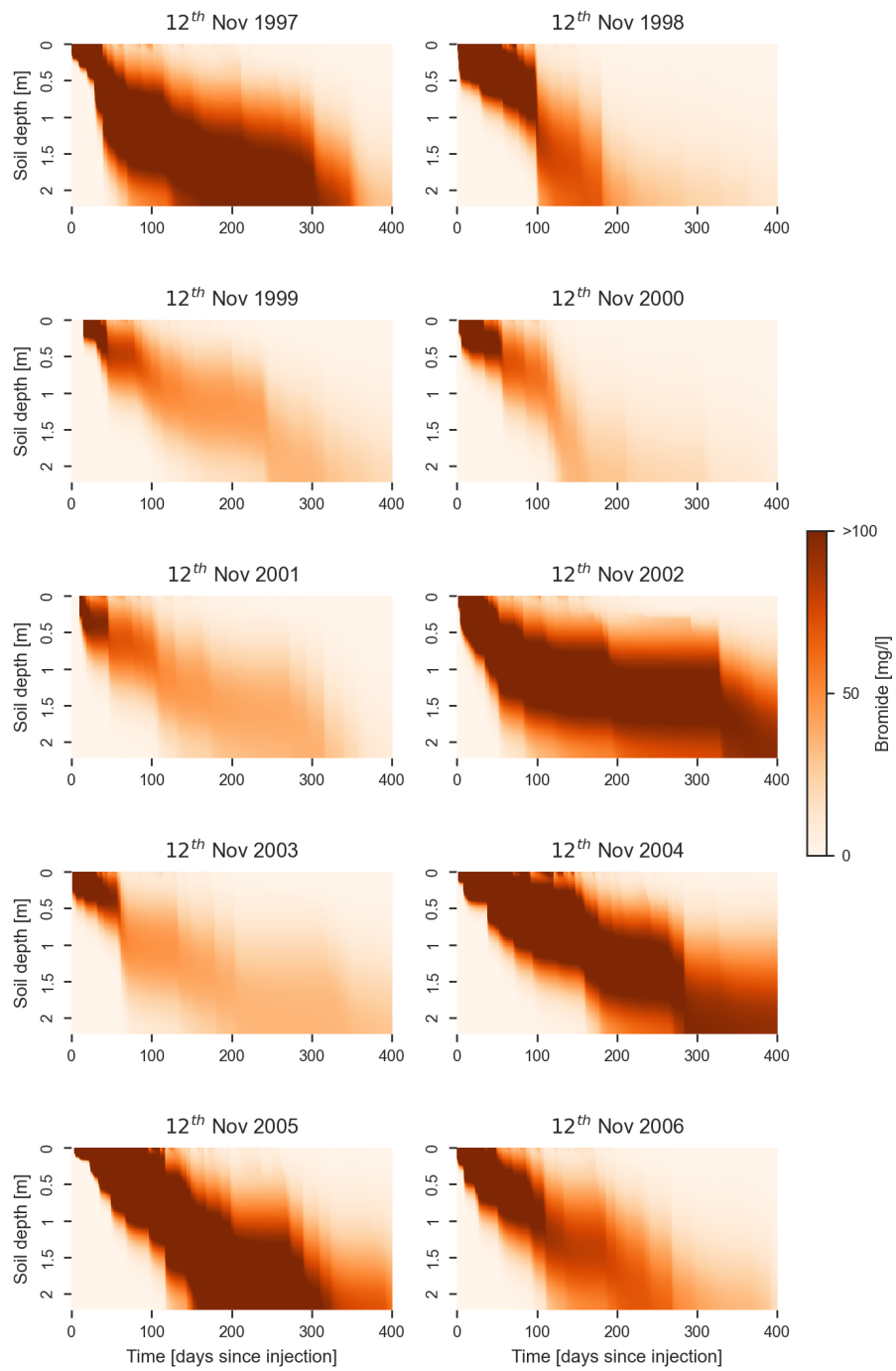
**Figure S17.** Simulated bromide concentrations of soil water with HYDRUS-1D
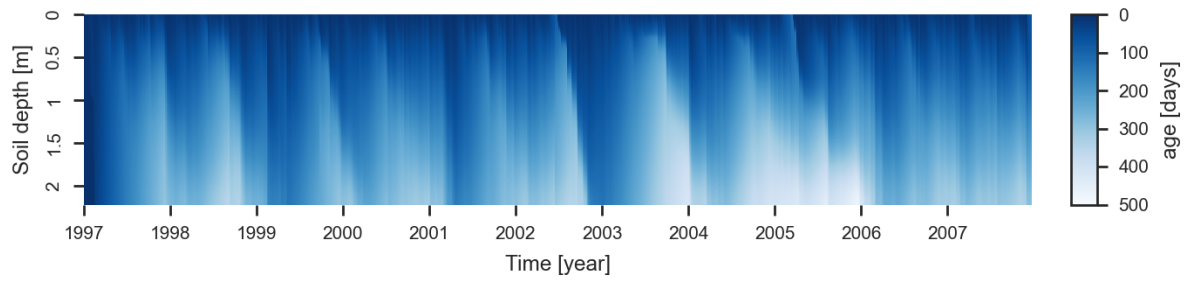
Figure S18. Mean residence time of soil water simulated with HYDRUS-1D.

Table S3. Parameters of HYDRUS-1D with dual-porosity domain

Model parameter		Unit	Parameter boundaries	Best parameter
Vertical discretization	Δz	cm	2	2
Soil depth	z_{soil}	cm	220	220
Effective porosity	θ_{eff}	-	0.15 - 0.65	0.47
Fraction of mobile region	f_m	-	0.01 - 0.99	0.86
Fraction of immobile region	f_{im}	-	$1 - f_m$	0.14
Residual water content for the mobile region	θ_r^m	-	0	0
Saturated water content for the mobile region	θ_s^m	-	$\theta_{eff} \cdot f_m$	0.40
Parameter in the soil water retention function	$alfa$	cm^{-1}	0.001 - 0.1	0.04
Exponent in the soil water retention function	n	-	1.01 - 2.3	1.07
Saturated hydraulic conductivity	k_s	cm day^{-1}	2.4 - 360	200.9
Pore-connectivity parameter	l	-	0.5	0.5
Residual water content for the immobile region	θ_r^{im}	-	0	0
Saturated water content for the immobile region	θ_s^{im}	-	$\theta_{eff} \cdot f_{im}$	0.07
First-order rate coefficient in the water mass transfer equation	ω	day^{-1}	0.1 - 10	2.54
Bulk density of porous medium	ρ	$g\ cm^{-3}$	1.5	1.5
Longitudinal dispersivity	D_l	cm	0 - 40	7.55
Dimensionless fraction of the adsorption sites	f_{mo}	-	1	1
Physical nonequilibrium[a]		-	0	0

[a] Set equal to 0 when the physical nonequilibrium option is not considered.